Proceedings of the ASME 30th International Conference on Ocean, Offshore and Arctic Engineering

OMAE2011

June 19-24, 20111, Rotterdam, the Netherland

OMAE2011-50063

STRUCTURAL DESIGN OF A HORIZONTAL-AXIS TIDAL CURRENT TURBINE COMPOSITE BLADE

Gunjit Bir
National Renewable Energy Laboratory
Email: gunjit.bir@nrel.gov

Michael Lawson
National Renewable Energy Laboratory
Email: michael.lawson@nrel.gov

Ye Li
National Renewable Energy Laboratory
Email: ye.li@nrel.gov

ABSTRACT

This paper describes the structural design of a tidal turbine composite blade. The structural design is preceded by two steps: hydrodynamic design and determination of extreme loads. The hydrodynamic design provides the blade external shape, i.e. the chord and twist distributions along the blade, which result in optimal performance of the tidal turbine over its lifetime. The extreme loads, i.e. the extreme flap and edgewise loads that the blade would likely encounter over its lifetime, are associated with extreme tidal flow conditions and are obtained using a computational fluid dynamics software. Given the blade external shape and the extreme loads, we use laminate-theory-based structural design to determine the optimal layout of composite laminas such that the ultimate-strength and buckling-resistance criteria are satisfied at all points in the blade. The structural design approach allows for arbitrary specification of the chord, twist, and airfoil geometry along the blade and an arbitrary number of shear webs. Certain fabrication criteria, e.g. each composite laminate must be an integral multiple of its constituent ply thickness, are imposed. In the present effort, the structural design uses only static extreme loads; dynamic-loads-based fatigue design will be addressed in the future. Following the blade design, we compute the distributed structural properties, i.e. flap stiffness, edgewise stiffness, torsion stiffness, mass, moments of inertia, elastic-axis offset, and center-of-mass offset along the blade. Such properties are required by hydro-elastic codes to model the tidal current turbine and to perform modal, stability, loads, and response analyses.

INTRODUCTION

Extraction of energy from tidal currents, an untapped renewable resource so far, is gaining increased attention. Tidal currents are an attractive source of renewable energy due to their predictability and high energy density. Recently, numerous technologies have been developed to convert the energy available within tidal currents in to electrical power [1]. Horizontal-axis tidal turbines (HATTs) are perhaps the most mature and promising of the technologies and several companies (e.g. Marine Current Turbine, Verdant Power, and OpenHydro) have developed HATT prototypes that are currently undergoing testing. Nevertheless, as blade failures on a number of prototype devices have demonstrated, the ability to design HATT blades to withstand the expected hydrodynamic loads is critical. A HATT basically works on the same principle as does a horizontal-axis wind turbine. The HATT rotor blades convert the tidal current kinetic energy into the shaft mechanical energy and a generator converts this mechanical energy into electricity. Figure 1 shows a few examples of HATT configurations. These configurations differ in the type of support structure used for the turbine rotor. Fraenkel [1] discusses pros and cons of each configuration.

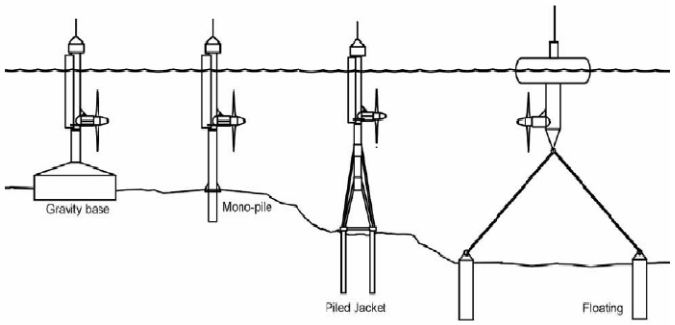

Figure 1. Examples of horizontal-axis tidal current turbine (HATT) configurations. Each configuration is best-suited for a particular sea depth range (Reference 1).

Irrespective of which configuration is used, the rotor blade is the key component that extracts energy from the tide and primarily dictates the performance, loads, and dynamics of the

whole turbine system. An efficient blade design is, therefore, critical to the success of the HATT.

This paper focuses on the structural design of a tidal turbine composite blade. The structural design is preceded by two steps: hydrodynamic design and determination of extreme loads. The hydrodynamic design, discussed in the companion paper [2], provides the blade external shape, i.e. the chord and twist distributions along the blade that result in optimal performance of the tidal turbine over its lifetime. The extreme loads, i.e. the extreme flap and edgewise loads that the blade would likely encounter over its lifetime, are associated with extreme tidal flow conditions and are determined using a computational fluid dynamics software. Given the blade external shape and the extreme loads, we use laminate-theory-based structural design to determine the optimal layout of composite laminas such that the ultimate-strength and buckling-resistance criteria are satisfied at all points in the blade. Our structural design approach allows for arbitrary specification of the chord, twist, and airfoil geometry along the blade and an arbitrary number of shear webs. Certain fabrication criteria, e.g. each composite laminate must be an integral multiple of its constituent ply thickness, are imposed. In the present effort, the structural design uses only static extreme loads; dynamic-loads-based fatigue design is not addressed. Following the blade design, we compute the distributed structural properties, i.e. flap stiffness, edgewise stiffness, torsion stiffness, mass, moments of inertia, elastic-axis offset, and center-of-mass offset along the blade. Such properties are required by hydro-elastic codes to model the tidal current turbine and to perform modal, stability, loads, and response analyses.

THE TIDAL CURRENT TURBINE DESCRIPTION

This paper considers a hypothetical monopole-supported 550 KW turbine shown in Figure 2; it is intended for deployment at the Northern Admiralty Inlet of Puget Sound. Table 1 lists the key design and operating specifications for the turbine.

Table 1. Turbine specifications

Rated power	550 kW
Number of rotors	2
Rotor diameter	20 m
Number of rotor blades	2
Control type	Variable speed, variable pitch
Hub diameter	2 m
Maximum rotor speed	11.5 rpm
Normal flow speed range	0.5-3.0 m/s
Hub height	18 m
Primary blade airfoil	NACA 63_1-424
Water depth	33 m

The turbine has two 20-meter diameter rotors. Each rotor has two blades and is mounted on a 2-meter diameter hub. The blade design is optimized for a variable-speed variable-pitch (VSVP) operation. A NACA 63_1-424 airfoil defines the primary shape of the turbine blade; this airfoil was selected because it provides a relatively large minimum pressure coefficient and makes the blade resistant to cavitation. Also, NACA 63 series airfoils delay stall and are less sensitive to leading edge roughness than NACA 4 and 5 series airfoils. We assume a circular cross-section over the blade root length that is well suited to variable- pitch mechanism. The circular section transitions to the NACA 63(1)-424 airfoil shape at 20% of the blade span. It may be possible to improve the performance of the blade (i.e. increase power generation) by using different airfoil shapes over the blade length. We will explore this possibility in the future.

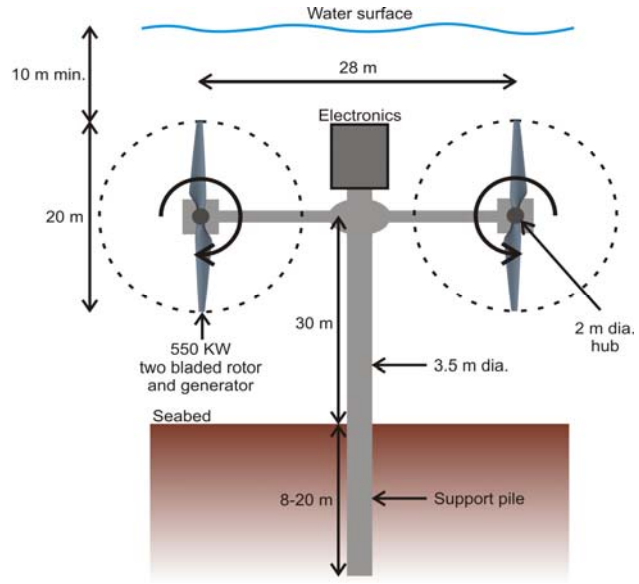

Figure 2a. Schematic of the monopole-supported tidal current turbine. The monopole is dug into the seabed and the twin rotor assembly can slide up and down the vertical shaft.

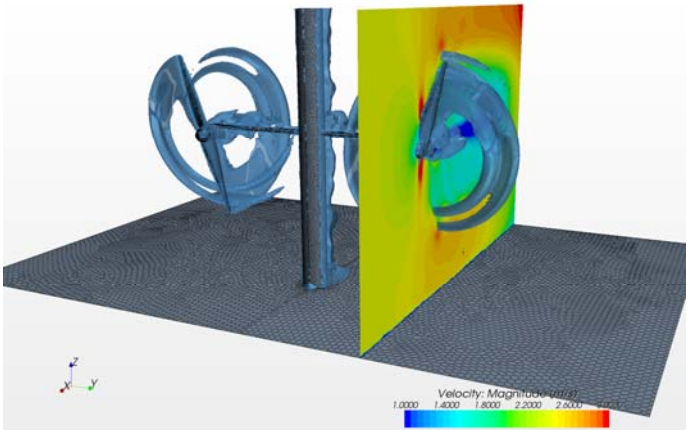

Figure 2b. Each rotor has two blades. The blades shed strong tip vortices, as shown in this CFD simulation, and significantly influence the blade loads.

DESIGN APPROACH

Figure 3 summarizes the hydro-structural design of the HATT blade and computation of its structural properties. The green boxes identify the three main steps, i.e. hydrodynamic design, computation of extreme loads, and structural design, and are described in following sections.

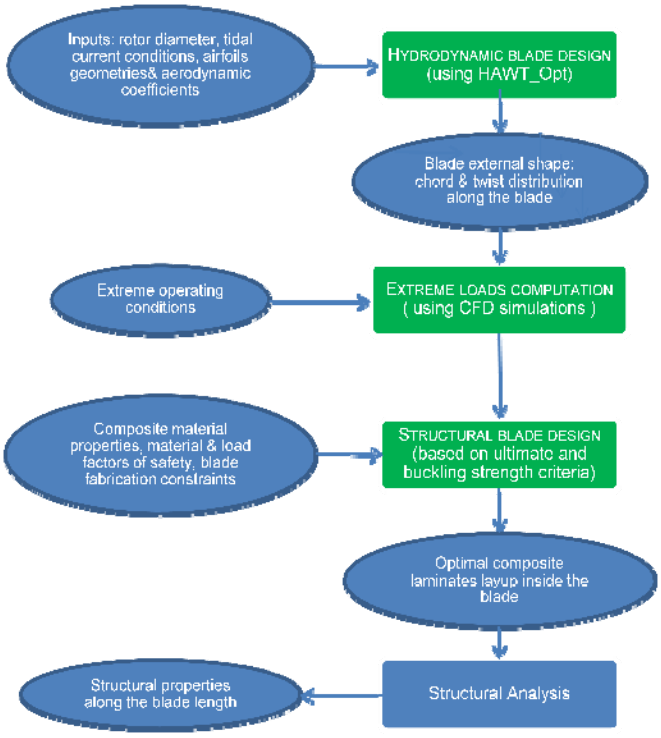

Figure 3. Steps used in the aero-structural blade design.

HYDRODYNAMIC DESIGN

The turbine blade is designed for a hypothetical 550 KW turbine intended for deployment at the Northern Admiralty Inlet of Puget Sound. An acoustic Doppler current profiler survey at this site [3] shows the mean water velocity is approximately 1 m/s, although velocities as high as 3 m/s occur during the tidal cycle. Table 1 presents the turbine's specifications. The turbine has a 20 m diameter rotor comprised of a 2 m diameter hub and two blades. The blade design is optimized for a variable-speed variable-pitch (VSVP) turbine that has a maximum rotation rate of 11.5 rpm.

We used our recently developed numerical tool Harp_Opt [4,5] for the basic turbine blade design. Harp_Opt combines the blade element moment code WT_Perf [6] with a genetic algorithm to provide optimal blade twist angle and chord distribution along the blade for a specified objective function. The optimization objective for our blade design was to maximize tidal energy capture over the flow speed range 0.5-3.0 m/s while limiting the turbine's maximum power output to 550 kW (the cavitation effects were ignored). Using this objective, Harp_Opt determined the blade chord and twist distribution along the blade (figure 4). Note that the blade span location, r, with respect to the hub center has been normalized by R, the rotor radius. Figure 5 shows the computed optimal tip-speed ratio, rotor rotation speed and optimal blade pitch angle for each tidal current velocity. The tip-speed ratio (TSR) is defined as the ratio of the rotor tip speed and the mean tidal flow speed. Figure 6 shows how the rotor thrust and the blade root flap moment vary with the tidal current velocity.

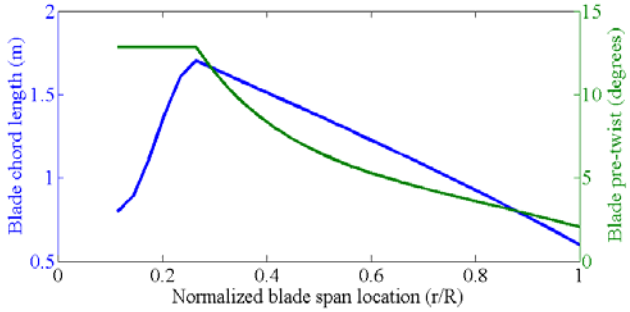

Figure 4. Optimal chord and twist distribution along the blade.

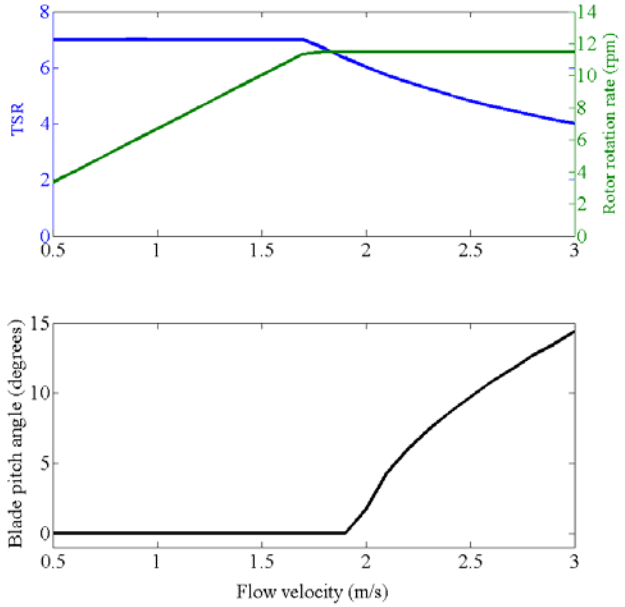

Figure 5. Variations of optimal tip-speed ratio (TSR), rotor speed, and blade pitch angle with tidal flow velocity.

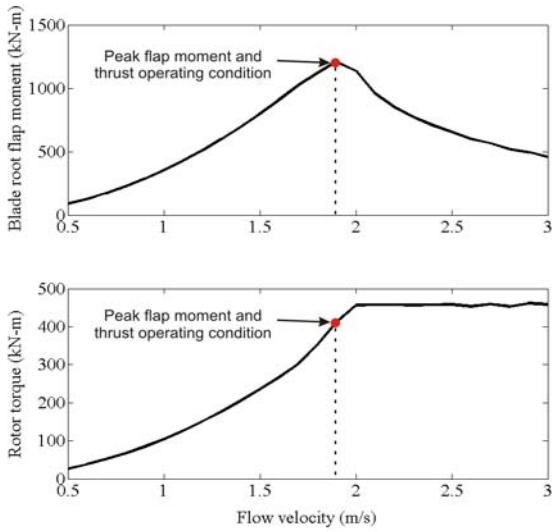

Figure 6. Variation of blade root flap moment and rotor torque with the tidal current velocity.

The chord and twist distribution, which HARP_Opt computed at thirty sections along the blade, define the external shape of the blade (figure 7).

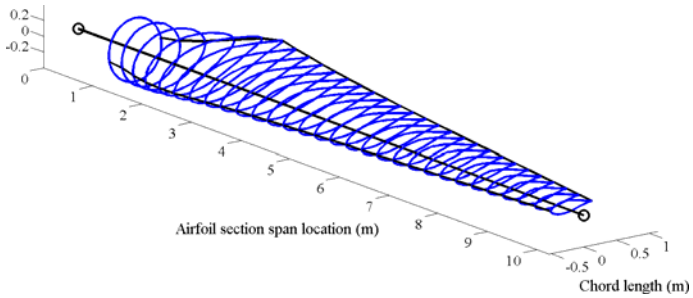

Figure 7. Airfoil chord and twist variation along the blade.

ESTIMATION OF EXTREME BLADE LOADS

Definition of extreme conditions

For structural design, we need to know the maximum loads the blade must withstand during its lifetime. We identified two extreme operating conditions during which the blade is expected to encounter maximum loads.

Extreme operating condition 1 (EOC1): The tidal current velocity becomes significantly higher than the normal velocity due to an extreme weather event. In this case, to prevent blade overloading, the turbine control system automatically feathers the blades and engages the shaft brake to prevent rotor rotation. For this condition, we assume that the tidal current can attain a velocity twice the maximum velocity measured during the normal tidal cycle in the Northern Admiralty Inlet. The maximum velocity during a normal tidal cycle is approximately 3 m/s at hub height. Thus we considered current velocities up to 6 m/s.

Extreme operating condition 2 (EOC2): The turbine is operating normally at the peak thrust and peak blade root flap moment operating condition (see Figure 6), which corresponds to 1.9 m/s tidal current speed, zero degree blade pitch angle, and 11.5 rotor rpm. The turbine then suddenly experiences a tidal gust due to the passage of a turbulent eddy that boosts the tidal current velocity to 2.85 m/s, which 1.5 times the normal current velocity. The turbine control system is unable to pitch the blades quickly enough to shed the increased hydrodynamic loading associated with this event. Recent experimental measurements from the Puget Sound [7] suggest that velocity increments larger that 50% occurs rarely on the length scale of the turbine blades. Therefore, our choice of 1.5 times the normal speed as the extreme tidal current speed is quite conservative.

Extreme loads computation

To obtain extreme hydrodynamic loads on the blade, we simulated the extreme operating condition, EOC1 and EOC2, using the CFD code STAR CCM+ (CD-Acapco; Melville, New York [8]). For these simulations we took advantage of the 180 degree periodicity of the turbine rotor and only simulated one blade and half of the hub. To simulate the rotation of the blade and the hub, we rotated the model reference frame; this approach effectively simulated blade rotation without the need to physically rotate the computational grid and forming the Navier-Stokes equations in a frame that is rotating with the turbine. Figure 8 shows the computational grid used for the CFD simulations.

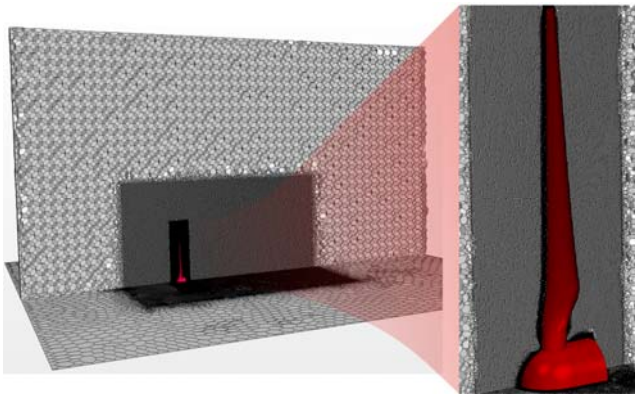

Figure 8. Computational grid used for CFD simulations.

A constant and spatially uniform velocity profile was specified over the front of the computational domain and a pressure outlet boundary condition was applied at the exit end. No-slip boundary conditions were applied on the surfaces of the blade and the hub. Turbulence was modeled using the k-ω SST (shear stress transport) Reynolds-averaged Navier-Stokes (RANS) sub-grid scale model. The computational grid was generated using the STAR CCM+ grid generation utility and consisted of approximately 3 million polyhedral elements. The RANS equations were solved using a second-order-accurate finite-volume discretization scheme via a segregated algebraic multi-grid iterative solver. Simulations were judged to be

converged when the residuals of the numerical solution stabilized and were reduced by approximately three orders-of-magnitude. Several global parameters, including rotor torque and thrust, were also monitored to insure convergence of the solution. Lawson et al [2] provide a more detailed description of the development and numerical verification of the CFD simulations.

The CFD simulations provide the flow field within the computational domain and also the blade pressure distribution (figure 9) corresponding to the extreme operating condition (EOC). Spatial integration of the pressure distribution yields extreme load distributions, specifically the shearing forces and the bending moments, over the blade.

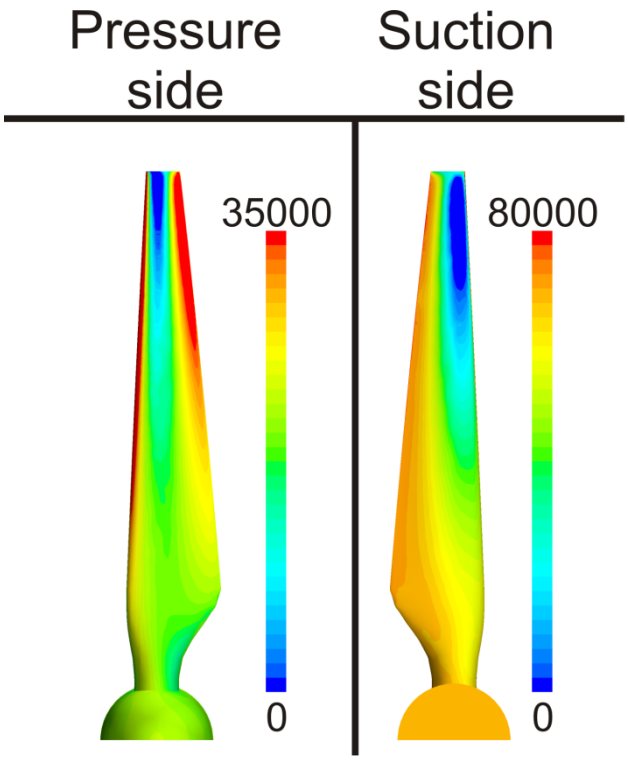

Figure 9. Blade pressure distributions for the extreme operating condition, EOC2. Units are in Pascals.

The structural design, described in the next section, considers only the flap and lag bending moments. Figure 10 shows the bending moment distributions along the blade for each EOC. These moments are first obtained in the global frame (shown in dotted lines). The global frame is a blade-section-attached frame, which does not twist with blade and stays parallel to a hub-attached frame with one axis aligned with the blade pitch axis and another normal to the rotor plane. The bending moments are then transformed to blade-section-attached local frame (shown in solid lines). The local frame has one axis aligned with the blade pitch axis and the other with the local chord line. Figure 10 indicates that both flap and lag bending moments are largest for EOC 2. Hydrodynamic loads from Scenario 2, referenced to the local section frames, were used to design the internal structure of the blade.

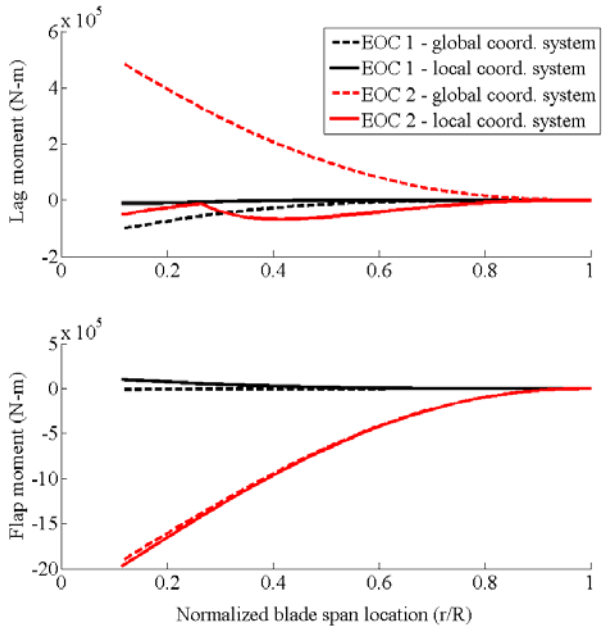

Figure 10. Flap and lag bending moments computed for the two extreme operating conditions, EOC 1 and EOC 2.

STRUCTURAL DESIGN AND ANALYSIS

For the HATT blade structural design, we use a computerized method that closely follows the one we developed earlier for the preliminary design of composite wind turbine blades [9]. The method allows for arbitrary specification of the chord, twist, and airfoil geometry along the blade and an arbitrary number of shear webs. Given the blade external geometry description and the design load distribution, the code uses ultimate-strength and buckling-resistance criteria to compute the optimal design thickness of load-bearing composite laminates at each blade span location. The code also includes an analysis option to obtain blade properties following blade design. These properties include bending stiffness, torsion stiffness, mass, moments of inertia, elastic-axis offset, and center-of-mass offset along the blade. Nonstructural materials—gelcoat, nexus, and bonding adhesive—are also included for computation of mass.

Figure 11 shows the assumed structural layout of composite materials within a typical blade cross section. The figure shows a three-cell blade section with two webs, but the code is applicable to a multi-cell section with an arbitrary number of webs. The outermost skin of a section consists of three layers: a gelcoat layer, a nexus layer, and a double-bias-material composite laminate. In this report, we define a laminate as a stack of plies, where a ply is a planar composite mat. The gelcoat outer layer provides a smooth surface, and although it is not a structural material, it can significantly contribute to the blade mass. Nexus is a soft-material mat that shields the rough surface of the underlying double-bias laminate and provides a

relatively smooth but absorbent surface for the gelcoat. At the blade trailing edge, the double-bias laminate splits into two layers to accommodate a core material, such as foam, or honeycomb, as shown in detail CC. The core-material laminate augments the buckling strength of the trailing section of the blade.

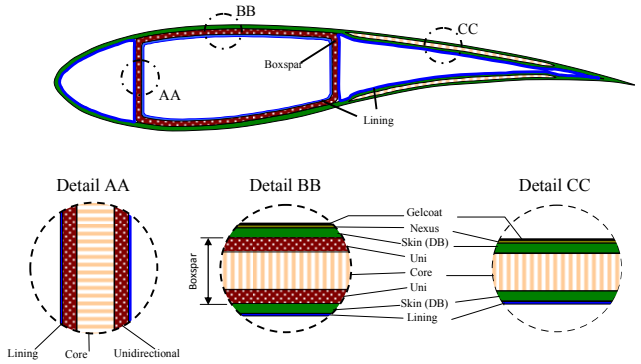

Figure 11. Structural layup of composite laminates at a typical blade section.

A composite box-spar runs along the midsection of the blade and is attached to the skin double-bias layers at its upper and lower surfaces. The box-spar divides the blade interior into three cells, with the box-spar forming the mid-cell. A lining, typically a double-bias layer, covers the inside surface of each cell. As shown in detail BB, the box-spar is made of unidirectional composite laminates with an embedded core material. Because of its good axial load-bearing capabilities, the unidirectional laminate provides most of the bending strength. The core material provides the buckling strength to the mid-cell. The two vertical sides of the box-spar serve as webs. Detail AA of Figure 11 shows the sequence of composite layers in each web.

Whereas the primary function of the unidirectional layers is to provide flexural strength, the functions of the double-bias layers are to provide shear strength and to prevent splaying of the unidirectional material. Computational effort is minimized by assuming that all double-bias plies are stacked in one laminate and all unidirectional plies are stacked in another laminate (detail BB in Figure 11). In reality, the double-bias and unidirectional plies may be interspersed to form a single laminate. This interspersing of plies may have a significant effect on the blade structural integrity at the micro level. However, it will have little effect on the blade strength and properties predicted by the code, assuming the thickness of the combined stack is much smaller than the overall blade thickness, which usually is the case.

Figure 11 shows a box-spar configuration, which we used for our studies. A D-spar configuration may be obtained by simply moving the forward web to the leading-edge location, where its height automatically becomes zero. Depending on the loading environment and manufacturing considerations, a designer may opt for structural layouts different from the one shown in Figure 11. For example, for the webs, the designer might replace the unidirectional laminates with double-bias laminates, which provide higher shear strength. Some blade designs show the upper- and lower-surface unidirectional laminates extended somewhat beyond the web locations. Currently, we are surveying construction details of a few blades and consulting with tidal current blade designers to identify candidate layouts that are most likely to be used and we may extend our code to accommodate the additional layouts.

Technical approach

The design objective is to size the thickness of the unidirectional laminate, double-bias laminate, and core material such that the blade has minimum weight and remains fail-safe under the extreme load distribution. For a conservative design, we assume that the gelcoat and the nexus are not load-bearing materials and, therefore, are not sized. The design is carried out using the ultimate strength criterion, the buckling strength criterion, and two trend-based relations. Details are provided in Reference 9; a summary, however, is provided below.

To satisfy the ultimate strength criterion, we first develop laminate-theory-based mathematical expression that relates axial stress at any point within the blade to the loading and composite material elastic properties at that point. We then impose a constraint to ensure that this stress does not exceed the allowable design stress for the composite material at that point. The allowable design stress for the material is its ultimate strength, compressive or tensile, multiplied by a material factor of safety.

To satisfy the buckling criterion, we use the following inequality:

$$\int_{panel-bottom}^{panel-top} \sigma(z,\zeta,\tau)\,d\tau \;\le\; 3.6 * \frac{\pi^2}{b^2} \int_{panel-bottom}^{panel-top} \frac{E(z,\zeta,\tau)\tau^2}{[1-(\upsilon(z,\zeta,\tau)^2)]} d\tau$$

It states that the edge loading per unit peripheral length of a blade surface panel does not exceed the Euler buckling load for that panel. The left-hand side of this equation expresses the edge loading per unit peripheral length of a blade surface panel and it is obtained by integrating the axial compressive stresses over the thickness of a panel. The longitudinal z-axis is directed toward the blade tip and the ζ- and the τ-axes form the mid-surface of the panel. The τ represents the distance of a material point in the panel from the z-ζ neutral surface. The right-hand side of equation (1) represents the critical buckling load of the panel (note that it is proportional to the panel flexural rigidity represented by the integral term on the right-hand side). E is the effective Young's modulus in the longitudinal z direction and ν is the Poison's ratio at the point (z,ζ,τ). We apply the buckling criterion to the mid-panel, which is the blade upper surface enclosed between the fore- and aft-webs, and to the trailing-edge panel, which is the blade upper surface enclosed between the aft-web and the trailing edge. The highly curved and short-length leading-edge panel is assumed to be buckle-

free. For a conservative buckling analysis, we assume the panel edges parallel to the z-axis are simply supported, and the edges perpendicular to the z-axis are free. In reality, all edges would have a finite restraint to rotation due to the adjoining panels, and the buckling resistance would be somewhat enhanced. Also to keep the analysis simple, we ignore the nonlinear geometric and inelastic effects.

Compared to unidirectional-material, the double-bias material usually offers a much lower stiffness along the blade. The ultimate-strength criterion would, therefore, dictate that only the unidirectional-material be used resulting in a zero-thickness requirement for the double-bias material. Though the double-bias material does contribute to flexural rigidity, its prime role is to prevent splaying of the unidirectional plies, provide resistance to accidental denting of the blade surface, and provide shear strength. Because of the low torsion loads likely to be encountered by a typical wind blade, the shear-strength criteria also may not yield any requirement for the double-bias material. A rigorous relation governing double-bias material requirement for splay-prevention and dent-resistance is not available. We, therefore, consulted wind turbine blade designers and manufacturers and their input helped us formulate the following simple relation to compute the double-bias laminate thickness:

$$t_{db} = \max[mtsbypw * \max(w_{panel-1}, w_{panel-2}, \cdots, w_{panel-n}), mdbplies * t_{db-ply}]$$

where *wpanel-i* is the width of panel *i* between webs *i* and *i+1*, *tdb-ply* is the ply thickness of the double-bias material, *mdbplies* is the minimum number of double-bias plies, and *mtsbypw* is the minimum double-bias-laminate-to-panel-width ratio. For *mdbplies* and *mtsbypw*, we used the values 3 and 0.0025 respectively. These are typical values for the 10-meter long wind turbine blades, but may be inadequate for similar size marine turbine blades because of the crushing or impact loads from the surrounding water. We plan to consult marine blade designers to provide us with specific guidelines.

After satisfying the ultimate and buckling strength criteria described above, we increased the laminate thickness in the root area to allow secure attachment of the blade to the hub (see Reference for details). We also impose the design requirements that the thickness of any laminate is an integer multiple of the thickness of the commercially available composite ply sheet.

Finally, we consider a filler material for the blade interior. Unlike a wind turbine blade, a marine turbine blade experiences substantial buoyancy forces due to the surrounding dense water. These forces act along the full length of the blade. Also, the direction of these large forces changes cyclically per each blade revolution resulting in fatigue damage. To minimize these cyclic forces, the blade should be made as neutrally buoyant as possible. Researchers have suggested filling the blade interior with water or with epoxy slurry whose density is close to that of the water.

Computation of structural properties

Using the composite laminates layup that results from the structural design, we compute the following structural properties along blade length: mass per unit length (m), flap stiffness (EI_{flap}), lag stiffness (EI_{lag}), axial stiffness (EA), torsion stiffness (GJ), and offsets of the elastic-axis (x_ea) and center-of-mass (x_cg) from the blade pitch axis. Each of these properties is a span-variant section property and is obtained by integrating either the materials density or the materials elastic parameters distributed over a specific section. The integral relations are quite simple and follow directly from the elementary mechanics of materials [10]. It may be mentioned that we ignore the effect of warping in the current formulation. In the near future, we plan to introduce Vlasov's correction to account for the warping effects; this would yield improved estimates of torsion stiffness, particularly near the root area.

For computer evaluation of the various integrals that provide the structural properties, we discretize all the section laminates into a number of area segments along each section periphery. Based on the segment area, its distance and orientation with respect to the ξ- and η-axes, and the elastic moduli of the material enclosed by it, we determine its contribution to a particular section property. Contribution of all material segments is then added to yield the gross section property. In computing blade properties, we include the mass of the nonstructural materials, including gelcoat, nexus, and bonding adhesive. Also, at the blade root section, we take into account the mass contribution of bolts [9].

RESULTS

Design

To design the tidal current turbine composite blade, we followed steps outlined in the previous section. We first used HARP_Opt and obtained the blade external hydrodynamic shape, i.e. airfoil chord and twist distribution along the blade (figure 4). The blade is 8.85-meter long and has a circular cross section at the root with a diameter of 0.8 meter. From the root to the 2.4-meter span location, the blade section transitions from the circular shape into the NACA 63_1-424 airfoil shape. Outboard of this span location, the airfoil shape remains unchanged.

Table 2. Blade material properties

Material	t_{ply} (mm)	ρ (Kg/m^3)	E (Pa)	G (Pa)	σ_{ut} (Pa)	σ_{uc} (Pa)	ν
Gelcoat	0.381	1664	--	--	--	--	--
Nexus	0.51	1830	--	--	--	--	--
Double-Bias	0.53	1830	10.3E+9	8.0E+9	151	-174	0.3
Lining	0.53	1830	10.3E+9	8.0E+9	151	-174	0.3
Unidirectional	0.53	1860	37.0E+9	4.1E+9	986	-746	0.3
Core	3.125	128.1	--	--	--	--	0.3

Next, we defined extreme operating conditions and, using a CFD code, computed the maximum loads the blade would encounter during its lifetime (figure 10). Then we selected material properties using Reference 11 and other handbooks. Table 2 lists the material properties: t_{ply} is the composite ply

thickness, ρ is the material density, E is the effective modulus of elasticity in a direction parallel to the blade longitudinal axis, G is the shear modulus, σ_{ut} is the ultimate allowable tensile stress, σ_{uc} is the ultimate allowable compressive stress, and ν is material the Poisson's ratio. The ultimate stresses are the mean values from coupon testing [11]. We applied a safety factor of 1.2 to the loads and a safety factor of 1.5 to the materials (to arrive at the allowable design stresses).

Next, we performed structural design, the final step in the design process, which yielded minimal thicknesses of the composite laminates and optimal location of the boxspar webs such that minimal material is used while satisfying the ultimate and buckling strength criteria.

Table 3 shows the design thicknesses of composite laminates required at 74 sections along the blade. The optimal web locations are 12.8% and 56.0% of the chord length. The first column lists the blade section numbers and the second column lists the span location of those sections. The third column lists the chord lengths. The *tsk*, listed in next column, is the design thickness of the double-bias skin material required at different blade stations. This thicknesses needs to be augmented such that it becomes an integer multiple of the commercially available double-bias composite ply. The *tskn* and *nskin*, listed in the next two columns, represent the augmented skin-laminate thickness and the number of plies required to obtain that thickness. The next three columns, with the headers *tecore*, *tecoren*, and *ntecore*, represent similar values for the core material (PVC foam) required at the blade trailing edge for resistance against buckling. The subsequent three columns, with the headers *tuni*, *tunin*, and *nuni*, represent corresponding values for the unidirectional material required in the box section. It is the unidirectional material that provides majority of the bending stiffness and primarily meets the ultimate strength requirement. The *tboxcore* and *ncore_bx* represent the core-material thickness and the number of core plies required in the box spar to meet the buckling strength criterion. The *t_le*, *t_box*, and *t_te*, listed in the last three columns, respectively represent the blade section wall thickness at its leading edge, mid section (spanned by the box spar), and trailing edge parts. The wall thickness at any point on the blade surface is the sum of the thickness of gelcoat, nexus and all composite laminas at that point.

It should be noted that additional unidirectional and double-bias materials are used over the inboard blade span for blade root reinforcement. This reinforcement is required to accommodate bolt inserts for blade attachment to the hub, to mitigate stress concentrations, and to provide smooth stress flow paths from the blade to the hub [reference 9 provides an empirical formula for the root design]. The thickness of the reinforcement materials remains constant over a certain distance length from the blade root and then linearly tapers over the transition length, i.e., the length over which the blade section transitions from the circular shape to the regular airfoil shape. No core material is used over this blade-root region.

A close examination of the design results, listed in table 3, suggests that the leading edge wall thickness might too small for a tidal current turbine blade. While the shown thickness values are sufficient to meet the design criteria considered in the paper, these may not be adequate to withstand the crushing or impact loads from the water surrounding the blade. We are searching for specific design guidelines to address this issue.

Finally, to make the blade near-neutrally buoyant, we consider water or epoxy slurry to fill the blade interior. A filler agent also helps reduce the fatigue-causing cyclic loads on the blade as discussed earlier. Though a filler does not contribute to the blade strength, it substantially increases the blade mass. The filler material also might mitigate buckling and crushing of the blade due to surrounding water; however, we did not consider these in our design.

Structural properties

Next, using the composite layup that resulted from the blade design, we computed the span-variant structural properties. Table 3 lists these properties. The *m* is the mass per unit length; I_{xx} is the section mass moment of inertia about the chord; I_{yy} is the section mass moment of inertia about any axis normal to the chord and originating from the pitch axis; EI_{flap} is the flap stiffness; EI_{lag} is the lag stiffness or edgewise stiffness; *EA* is the axial stiffness; *GJ* is the torsion stiffness; *x_ea* is the offset of the elastic-axis from the blade pitch axis; and *x_ea* is the offset of the from the blade pitch axis. These offsets are positive if measured from the pitch axis toward the section leading edge. Note that the edgewise and torsion stiffness values dip around the 1.5-meter span location. This is because both these stiffness values are sensitive to the chord length (these are nearly proportional to the cube of the chord). Moving inboard from this location, the chord length reduces and so do the edgewise and the torsion stiffness values. Further inboard, the chord is the diameter of a circular section and remains constant, but the root reinforcement contributes substantially to the stiffness values. The slight dips in the mass and mass-inertia distribution seen in the table can be interpreted similarly (mass is roughly proportional to chord and mass-inertia is nearly proportional to the cube of the chord).

Table 5 provides a mass breakdown of the different materials used in the blade design. The contribution of mass of the bolt inserts and the filler material, though shown in the weight breakdown, is not included in section mass and inertia distributions shown in table 4. The inserts behave more like a concentrated mass at the discreet root location rather than a distributed mass reflected in the tables

After we account for the volume of the structural materials, the blade is left with a void of 24.9 m^3 in its interior. We consider two options: filling the interior with water and with epoxy slurry to achieve near-neutral buoyancy. The blade weight increases by 2402.7 kg if water is considered, by 2483.5 kg if epoxy slurry is considered. The resulting blade total weight becomes 2932.5 kg for water filler and 3213.2 kg for epoxy slurry filler (see table 5).

CONCLUSIONS AND FUTURE WORK

We presented results of the preliminary structural design of a horizontal-axis tidal turbine composite blade. The results show the optimal location of webs and the minimum thickness requirement of different composite laminates that would satisfy the ultimate strength and buckling resistance criteria. We considered only the extreme static loads that the blade would likely encounter during its lifetime. Dynamic loads, fatigue and criteria will be considered in the future.

A close examination of the design results showed that the leading edge wall thickness, while adequate to meet the buckling and strength criteria, might too small to withstand the crushing or impact loads from the water surrounding the blade. We are searching for specific design guidelines to address this issue.

Our design approach allows arbitrary twist, chord, and airfoil shape variation along the blade, but allows only a muliti-cell boxspar. Though a boxspar has been the choice by several HATT designers, we plan to extend our design code to accommodate a few more promising layouts. The materials we considered for the HATT design also appear adequate; however, we will critically assess a more materials, which may be more suitable for HATT blades.

In the current preliminary design approach, we ignored warping and section in-plane distortion (Brazier effect). We have developed a code called PreComp [12], which accounts for these effects and also allows for arbitrary layup of composite laminates within the blade. However, its present capability is limited to computation of structural properties only. We plan to extend it to compute 3D stresses and allow automated design. Following a PreComp-assisted preliminary design, we will use a finite-element based analysis, using NuMad [13] for example, to refine our blade design and obtain more accurate 3D stress field.

REFERENCES

[1] Fraenkel, P., 2002. “Power from marine currents”. Proceedings of the Institution of Mechanical Engineers, Part A: Journal of Power and Energy, 216(1), pp. 1–14

[2] Lawson, M.J., Li, Y., and Sale, D. C., 2011. “Development and verification of a computational fluid dynamics model of a horizontal axis tidal current turbine.” The 30th International Conference on Ocean, Offshore and Arctic Engineering.

[3] Polagye, B., and Thomson, J., 2010. Tidal energy reference model inflow conditions. Technical report.

[4] Sale, D. C., and Li, Y., 2010. “Preliminary results from a design methodology and optimization code for horizontal axis wind and hydrokinetic turbines.” The 29th International Conference on Ocean, Offshore and Arctic Engineering.

[5] NWTC Design Code Harp_Opt, available at http://wind.nrel.gov/designcodes/simulators/HARP_Opt/

[6] NWTC Design Code WT_Perf, available at http://wind.nrel.gov/designcodes/simulators/wtperf/

[7] Thomson J., Polagye, B., Richmond, M., and Durgesh, V. Quantifying turbulence for tidal power applications, MTS/IEEE Oceans 2010, Seattle, WA September 20-23, 2010.

[8] CD-Adapco, 2011, STAR CCM+ 5.06 User’s Guide.

[9] Bir, G.S. and Migliore, P., “A Computerized Method for Preliminary Structural Design of Composite Wind Turbine Blades.” Special November 2001 Wind Issue of the Journal of Solar Engineering. Also presented at the 2001 AIAA/ASME Wind Energy Symposium, Reno.

[10] Hodges, D.H. and Dowell, E.H., 1974, “Nonlinear Equations of Motion for the Elastic bending and Torsion of Twisted Nonuniform Rotor Blades,” NASA TN D-7818.

[11] Mandell, J.F. and Samborsky, D.D., 1997, “DOE/MSU Composite Material Fatigue Database: Test Meth¬ods, Materials, and Analysis,” SAND97-3002, Sandia National Laboratories Albuquerque, NM.

[12] User's Guide to PreComp (Pre-Processor for Computing Composite Blade Properties), NREL Report No. TP-500-38929, 2006

[13] Laird, D.L., 2001, “NuMAD User’s Manual”, SAND2001-2375, Sandia National Laboratories Albuquerque, NM.

Table 3. Design thickness requirement for composite laminate at different blade sections

Station	sloc	chord	tsk	tskn	nskin	tecore	tecoren	ntecore	tuni	tunin	nuni	tboxcore	ncore_bx	t_le	t_box	t_te
	(m)	(m)	(mm)	(mm)	--	(mm)	(mm)	--	(mm)	(mm)	--	(mm)	--	(mm)	(mm)	(mm)
1	0	0.8	5.64	5.83	11	0.00	0.00	0	31.99	32.33	61	21.78	7	7.25	61.46	7.25
2	0.075	0.823	5.64	5.83	11	0.00	0.00	0	31.99	32.33	61	24.25	8	7.25	64.58	7.25
3	0.15	0.847	5.64	5.83	11	0.00	0.00	0	31.99	32.33	61	26.65	9	7.25	67.71	7.25
4	0.225	0.871	5.64	5.83	11	0.00	0.00	0	31.99	32.33	61	29.00	10	7.25	70.83	7.25
5	0.3	0.894	5.64	5.83	11	0.00	0.00	0	31.99	32.33	61	31.29	11	7.25	73.96	7.25
6	0.375	0.95	5.64	5.83	11	0.00	0.00	0	31.99	32.33	61	36.59	12	7.25	77.08	7.25
7	0.45	1.006	5.64	5.83	11	0.00	0.00	0	31.99	32.33	61	41.72	14	7.25	83.33	7.25
8	0.525	1.062	5.48	5.83	11	19.36	21.88	7	31.05	31.27	59	0.00	0	7.25	38.52	29.13
9	0.6	1.118	4.97	5.30	10	20.82	21.88	7	28.14	28.62	54	0.00	0	6.72	35.34	28.60
10	0.675	1.185	4.39	4.77	9	22.50	25.00	8	24.88	24.91	47	3.39	2	6.19	37.35	31.19
11	0.75	1.252	3.78	4.24	8	24.19	25.00	8	21.42	21.73	41	13.90	5	5.66	43.02	30.66
12	0.825	1.319	3.16	3.18	6	26.15	28.13	9	17.91	18.02	34	24.43	8	4.60	47.62	32.73
13	0.9	1.386	2.58	2.65	5	27.83	28.13	9	14.64	14.84	28	31.04	10	4.07	50.16	32.20
14	0.975	1.442	2.53	2.65	5	29.01	31.25	10	14.36	14.84	28	33.03	11	4.07	53.29	35.32
15	1.05	1.498	2.48	2.65	5	30.19	31.25	10	14.05	14.31	27	34.86	12	4.07	55.88	35.32
16	1.125	1.554	2.48	2.65	5	31.37	34.38	11	14.08	14.31	27	36.77	12	4.07	55.88	38.45
17	1.2	1.61	2.51	2.65	5	32.55	34.38	11	14.22	14.31	27	38.67	13	4.07	59.01	38.45
18	1.275	1.633	2.51	2.65	5	33.04	34.38	11	14.22	14.31	27	39.46	13	4.07	59.01	38.45
19	1.35	1.657	2.51	2.65	5	33.54	34.38	11	14.24	14.31	27	40.25	13	4.07	59.01	38.45
20	1.425	1.681	2.52	2.65	5	34.03	34.38	11	14.28	14.31	27	41.04	14	4.07	62.13	38.45
21	1.5	1.704	2.55	2.65	5	34.53	37.50	12	14.43	14.84	28	42.12	14	4.07	62.66	41.57
22	1.575	1.694	2.58	2.65	5	34.31	34.38	11	14.62	14.84	28	41.76	14	4.07	62.66	38.45
23	1.65	1.683	2.62	2.65	5	34.08	34.38	11	14.82	14.84	28	41.40	14	4.07	62.66	38.45
24	1.725	1.673	2.65	3.18	6	33.59	34.38	11	15.03	15.37	29	37.11	12	4.60	57.47	38.98
25	1.8	1.662	2.70	3.18	6	33.37	34.38	11	15.31	15.37	29	36.77	12	4.60	57.47	38.98
26	1.875	1.651	2.73	3.18	6	33.14	34.38	11	15.44	15.90	30	36.57	12	4.60	58.00	38.98
27	1.95	1.64	2.75	3.18	6	32.92	34.38	11	15.58	15.90	30	36.21	12	4.60	58.00	38.98
28	2.025	1.63	2.77	3.18	6	32.69	34.38	11	15.71	15.90	30	35.86	12	4.60	58.00	38.98
29	2.1	1.619	2.80	3.18	6	32.46	34.38	11	15.85	15.90	30	35.50	12	4.60	58.00	38.98
30	2.25	1.598	2.80	3.18	6	32.02	34.38	11	15.85	15.90	30	34.80	12	4.60	58.00	38.98
31	2.4	1.577	2.85	3.18	6	31.58	34.38	11	16.12	16.43	31	34.16	11	4.60	55.41	38.98
32	2.55	1.556	2.80	3.18	6	31.13	31.25	10	15.85	15.90	30	33.38	11	4.60	54.88	35.85
33	2.7	1.534	2.75	3.18	6	30.67	31.25	10	15.56	15.90	30	32.66	11	4.60	54.88	35.85
34	2.85	1.513	2.69	3.18	6	30.23	31.25	10	15.25	15.37	29	31.91	11	4.60	54.35	35.85
35	3	1.492	2.63	2.65	5	30.06	31.25	10	14.93	15.37	29	34.88	12	4.07	56.94	35.32
36	3.15	1.471	2.58	2.65	5	29.62	31.25	10	14.59	14.84	28	34.05	11	4.07	53.29	35.32
37	3.3	1.45	2.51	2.65	5	29.18	31.25	10	14.25	14.31	27	33.21	11	4.07	52.76	35.32
38	3.45	1.429	2.45	2.65	5	28.72	31.25	10	13.90	14.31	27	32.47	11	4.07	52.76	35.32
39	3.6	1.407	2.39	2.65	5	28.27	31.25	10	13.54	13.78	26	31.63	11	4.07	52.23	35.32
40	3.75	1.386	2.32	2.65	5	27.83	28.13	9	13.16	13.25	25	30.80	10	4.07	48.57	32.20
41	3.9	1.365	2.26	2.65	5	27.39	28.13	9	12.78	13.25	25	30.11	10	4.07	48.57	32.20
42	4.05	1.344	2.19	2.65	5	26.93	28.13	9	12.39	12.72	24	29.28	10	4.07	48.04	32.20
43	4.2	1.322	2.12	2.12	4	26.75	28.13	9	11.99	12.19	23	32.42	11	3.54	50.11	31.67
44	4.35	1.301	2.04	2.12	4	26.30	28.13	9	11.58	11.66	22	31.45	11	3.54	49.58	31.67
45	4.5	1.279	1.97	2.12	4	25.85	28.13	9	11.16	11.66	22	30.72	10	3.54	46.45	31.67
46	4.65	1.257	1.90	2.12	4	25.38	28.13	9	10.74	11.13	21	29.75	10	3.54	45.92	31.67
47	4.8	1.235	1.82	2.12	4	24.92	25.00	8	10.31	10.60	20	28.78	10	3.54	45.39	28.54
48	4.95	1.214	1.74	2.12	4	24.47	25.00	8	9.87	10.07	19	27.81	9	3.54	41.74	28.54
49	5.1	1.192	1.66	2.12	4	24.02	25.00	8	9.41	9.54	18	26.85	9	3.54	41.21	28.54
50	5.25	1.17	1.59	1.59	3	23.82	25.00	8	8.96	9.01	17	30.37	10	3.01	43.27	28.01
51	5.4	1.148	1.59	1.59	3	23.36	25.00	8	8.48	8.48	16	29.18	10	3.01	42.74	28.01
52	5.55	1.125	1.59	1.59	3	22.89	25.00	8	7.99	8.48	16	28.44	10	3.01	42.74	28.01
53	5.7	1.103	1.59	1.59	3	22.41	25.00	8	7.50	7.95	15	27.25	9	3.01	39.09	28.01
54	5.85	1.081	1.59	1.59	3	21.94	25.00	8	7.01	7.42	14	26.06	9	3.01	38.56	28.01
55	6	1.058	1.59	1.59	3	21.47	21.88	7	6.51	6.89	13	24.86	8	3.01	34.90	24.89
56	6.15	1.035	1.59	1.59	3	20.98	21.88	7	6.01	6.36	12	23.64	8	3.01	34.37	24.89
57	6.3	1.012	1.59	1.59	3	20.50	21.88	7	5.51	5.83	11	22.41	8	3.01	33.84	24.89
58	6.45	0.989	1.59	1.59	3	20.01	21.88	7	5.00	5.30	10	21.17	7	3.01	30.19	24.89
59	6.6	0.966	1.59	1.59	3	19.53	21.88	7	4.50	4.77	9	19.92	7	3.01	29.66	24.89
60	6.75	0.943	1.59	1.59	3	19.04	21.88	7	3.99	4.24	8	18.65	6	3.01	26.00	24.89
61	6.9	0.92	1.59	1.59	3	18.56	18.75	6	3.49	3.71	7	17.37	6	3.01	25.47	21.76
62	7.05	0.896	1.59	1.59	3	18.05	18.75	6	3.01	3.18	6	16.05	6	3.01	24.94	21.76
63	7.2	0.872	1.59	1.59	3	17.55	18.75	6	2.53	2.65	5	14.71	5	3.01	21.29	21.76
64	7.35	0.848	1.59	1.59	3	17.04	18.75	6	2.06	2.12	4	13.35	5	3.01	20.76	21.76
65	7.5	0.824	1.59	1.59	3	16.54	18.75	6	1.61	2.12	4	12.91	5	3.01	20.76	21.76
66	7.65	0.8	1.59	1.59	3	16.03	18.75	6	1.18	1.59	3	11.57	4	3.01	17.10	21.76
67	7.8	0.776	1.59	1.59	3	15.53	15.63	5	0.77	1.06	2	10.25	4	3.01	16.57	18.64
68	7.95	0.751	1.59	1.59	3	15.00	15.63	5	0.40	0.53	1	9.20	3	3.01	12.92	18.64
69	8.1	0.726	1.59	1.59	3	14.47	15.63	5	0.41	0.53	1	8.86	3	3.01	12.92	18.64
70	8.25	0.701	1.59	1.59	3	13.95	15.63	5	0.50	0.53	1	8.52	3	3.01	12.92	18.64
71	8.4	0.676	1.59	1.59	3	13.42	15.63	5	0.41	0.53	1	8.17	3	3.01	12.92	18.64
72	8.55	0.651	1.59	1.59	3	12.89	15.63	5	0.58	1.06	2	8.38	3	3.01	13.45	18.64
73	8.7	0.626	1.59	1.59	3	12.37	12.50	4	0.57	1.06	2	8.00	3	3.01	13.45	15.51
74	8.85	0.601	1.59	1.59	3	11.84	12.50	4	0.65	1.06	2	7.63	3	3.01	13.45	15.51

Table 4. Variation of structural properties along the blade length

radius (m)	chord (m)	twist (deg)	m kg/m	Iyy kg-m	Ixx kg-m	x_cg (m)	x_ea (m)	GJ MN-m^2	EA MN	EI_{lag} MN-m^2	EI_{flap} MN-m^2
0	0.8	12.86	204.67	1.28E+01	1.47E+01	0	0	7.09E+07	3.17E+09	2.52E+08	2.43E+08
0.075	0.823	12.86	208.4	1.37E+01	1.50E+01	-0.003	-0.003	7.37E+07	3.21E+09	2.69E+08	2.47E+08
0.15	0.847	12.86	211.61	1.45E+01	1.51E+01	-0.007	-0.007	7.60E+07	3.24E+09	2.84E+08	2.47E+08
0.225	0.871	12.86	214.67	1.54E+01	1.51E+01	-0.01	-0.01	7.81E+07	3.27E+09	3.00E+08	2.46E+08
0.3	0.894	12.86	217.58	1.63E+01	1.50E+01	-0.014	-0.014	8.00E+07	3.30E+09	3.15E+08	2.44E+08
0.375	0.95	12.86	225.16	1.87E+01	1.55E+01	-0.024	-0.024	8.70E+07	3.40E+09	3.59E+08	2.50E+08
0.45	1.006	12.86	233.16	2.12E+01	1.56E+01	-0.035	-0.035	9.33E+07	3.48E+09	4.03E+08	2.49E+08
0.525	1.062	12.86	170.33	5.00E+00	8.13E+00	0.054	0.076	5.42E+07	2.56E+09	1.12E+08	1.70E+08
0.6	1.118	12.86	157	4.98E+00	7.25E+00	0.045	0.069	5.11E+07	2.34E+09	1.11E+08	1.48E+08
0.675	1.185	12.86	143.82	4.96E+00	6.64E+00	0.032	0.058	4.92E+07	2.07E+09	1.10E+08	1.30E+08
0.75	1.252	12.86	132.24	4.92E+00	6.00E+00	0.017	0.045	4.68E+07	1.83E+09	1.07E+08	1.12E+08
0.825	1.319	12.86	114.73	4.64E+00	4.97E+00	0.004	0.032	3.95E+07	1.52E+09	9.56E+07	8.82E+07
0.9	1.386	12.86	100.4	4.28E+00	4.05E+00	-0.014	0.017	3.47E+07	1.25E+09	8.55E+07	6.72E+07
0.975	1.442	12.86	102.79	4.51E+00	3.96E+00	-0.03	0.003	3.66E+07	1.25E+09	9.15E+07	6.45E+07
1.05	1.498	12.86	102.57	4.58E+00	3.80E+00	-0.047	-0.013	3.82E+07	1.22E+09	9.53E+07	6.00E+07
1.125	1.554	12.86	103.84	4.65E+00	3.60E+00	-0.066	-0.029	4.01E+07	1.22E+09	1.01E+08	5.62E+07
1.2	1.61	12.86	105.25	4.70E+00	3.38E+00	-0.085	-0.047	4.21E+07	1.22E+09	1.06E+08	5.17E+07
1.275	1.633	12.86	105.32	4.66E+00	3.24E+00	-0.094	-0.054	4.28E+07	1.21E+09	1.08E+08	4.94E+07
1.35	1.657	12.86	105.35	4.60E+00	3.10E+00	-0.102	-0.062	4.36E+07	1.21E+09	1.10E+08	4.70E+07
1.425	1.681	12.86	106.24	4.58E+00	2.97E+00	-0.111	-0.07	4.44E+07	1.21E+09	1.12E+08	4.45E+07
1.5	1.704	12.86	108.87	4.61E+00	2.86E+00	-0.119	-0.077	4.56E+07	1.24E+09	1.16E+08	4.30E+07
1.575	1.694	12.53	107.1	4.48E+00	2.72E+00	-0.118	-0.076	4.44E+07	1.23E+09	1.13E+08	4.09E+07
1.65	1.683	12.2	105.97	4.35E+00	2.59E+00	-0.117	-0.075	4.32E+07	1.21E+09	1.10E+08	3.89E+07
1.725	1.673	11.87	108.92	4.05E+00	2.54E+00	-0.122	-0.077	4.75E+07	1.26E+09	1.15E+08	3.84E+07
1.8	1.662	11.54	107.65	3.91E+00	2.40E+00	-0.121	-0.076	4.62E+07	1.24E+09	1.12E+08	3.62E+07
1.875	1.651	11.265	108.63	3.93E+00	2.34E+00	-0.119	-0.075	4.54E+07	1.26E+09	1.11E+08	3.57E+07
1.95	1.64	10.99	107.57	3.81E+00	2.24E+00	-0.118	-0.074	4.42E+07	1.25E+09	1.09E+08	3.41E+07
2.025	1.63	10.715	106.51	3.70E+00	2.14E+00	-0.118	-0.074	4.31E+07	1.24E+09	1.06E+08	3.26E+07
2.1	1.619	10.44	105.46	3.59E+00	2.05E+00	-0.117	-0.073	4.20E+07	1.22E+09	1.03E+08	3.11E+07
2.25	1.598	9.97	103.75	3.42E+00	1.92E+00	-0.116	-0.072	4.02E+07	1.20E+09	9.84E+07	2.91E+07
2.4	1.577	9.5	102.8	3.28E+00	1.77E+00	-0.113	-0.07	3.85E+07	1.21E+09	9.54E+07	2.72E+07
2.55	1.556	9.105	98.97	3.05E+00	1.66E+00	-0.113	-0.07	3.67E+07	1.16E+09	8.96E+07	2.54E+07
2.7	1.534	8.71	97.6	2.93E+00	1.59E+00	-0.112	-0.069	3.52E+07	1.14E+09	8.59E+07	2.43E+07
2.85	1.513	8.365	94.46	2.71E+00	1.49E+00	-0.111	-0.068	3.35E+07	1.09E+09	8.06E+07	2.26E+07
3	1.492	8.02	90.61	2.78E+00	1.40E+00	-0.104	-0.064	2.86E+07	1.06E+09	7.34E+07	2.15E+07
3.15	1.471	7.725	86.87	2.54E+00	1.30E+00	-0.104	-0.064	2.72E+07	1.01E+09	6.87E+07	2.00E+07
3.3	1.45	7.43	83.9	2.35E+00	1.22E+00	-0.104	-0.064	2.58E+07	9.67E+08	6.42E+07	1.85E+07
3.45	1.429	7.17	82.66	2.24E+00	1.17E+00	-0.103	-0.063	2.46E+07	9.53E+08	6.14E+07	1.77E+07
3.6	1.407	6.91	79.74	2.07E+00	1.09E+00	-0.102	-0.063	2.33E+07	9.08E+08	5.72E+07	1.63E+07
3.75	1.386	6.68	75.71	1.88E+00	1.00E+00	-0.103	-0.062	2.21E+07	8.63E+08	5.33E+07	1.50E+07
3.9	1.365	6.45	74.56	1.79E+00	9.58E-01	-0.101	-0.062	2.11E+07	8.50E+08	5.09E+07	1.43E+07
4.05	1.344	6.245	71.78	1.64E+00	8.90E-01	-0.101	-0.061	1.99E+07	8.07E+08	4.73E+07	1.32E+07
4.2	1.322	6.04	66.81	1.62E+00	8.07E-01	-0.095	-0.058	1.64E+07	7.50E+08	4.12E+07	1.19E+07
4.35	1.301	5.86	64.17	1.48E+00	7.48E-01	-0.095	-0.058	1.54E+07	7.09E+08	3.81E+07	1.09E+07
4.5	1.279	5.68	62.49	1.39E+00	7.03E-01	-0.094	-0.057	1.47E+07	6.97E+08	3.62E+07	1.04E+07
4.65	1.257	5.515	59.92	1.26E+00	6.48E-01	-0.093	-0.057	1.38E+07	6.57E+08	3.33E+07	9.42E+06
4.8	1.235	5.35	56.94	1.15E+00	5.97E-01	-0.093	-0.056	1.29E+07	6.18E+08	3.06E+07	8.54E+06
4.95	1.214	5.2	53.91	1.02E+00	5.42E-01	-0.094	-0.056	1.21E+07	5.81E+08	2.81E+07	7.73E+06
5.1	1.192	5.05	51.54	9.14E-01	4.98E-01	-0.094	-0.056	1.13E+07	5.44E+08	2.58E+07	6.97E+06
5.25	1.17	4.91	47.2	9.09E-01	4.42E-01	-0.087	-0.052	8.90E+06	4.95E+08	2.17E+07	6.17E+06
5.4	1.148	4.77	44.95	8.16E-01	4.03E-01	-0.087	-0.052	8.28E+06	4.60E+08	1.97E+07	5.51E+06
5.55	1.125	4.64	44.07	7.69E-01	3.80E-01	-0.086	-0.051	7.80E+06	4.51E+08	1.85E+07	5.19E+06
5.7	1.103	4.51	41.33	6.69E-01	3.40E-01	-0.086	-0.051	7.24E+06	4.17E+08	1.68E+07	4.61E+06
5.85	1.081	4.385	39.2	5.92E-01	3.07E-01	-0.086	-0.051	6.70E+06	3.85E+08	1.51E+07	4.07E+06
6	1.058	4.26	36.22	5.10E-01	2.73E-01	-0.087	-0.052	6.19E+06	3.53E+08	1.36E+07	3.57E+06
6.15	1.035	4.145	34.2	4.44E-01	2.45E-01	-0.088	-0.052	5.71E+06	3.23E+08	1.21E+07	3.11E+06
6.3	1.012	4.03	32.23	3.84E-01	2.19E-01	-0.088	-0.052	5.25E+06	2.93E+08	1.08E+07	2.69E+06
6.45	0.989	3.915	29.84	3.17E-01	1.92E-01	-0.089	-0.053	4.82E+06	2.65E+08	9.55E+06	2.31E+06
6.6	0.966	3.8	27.99	2.67E-01	1.70E-01	-0.09	-0.054	4.41E+06	2.37E+08	8.42E+06	1.96E+06
6.75	0.943	3.685	25.75	2.11E-01	1.47E-01	-0.092	-0.055	4.03E+06	2.11E+08	7.39E+06	1.65E+06
6.9	0.92	3.57	23.68	1.73E-01	1.29E-01	-0.093	-0.056	3.67E+06	1.85E+08	6.45E+06	1.37E+06
7.05	0.896	3.46	21.99	1.36E-01	1.13E-01	-0.094	-0.058	3.32E+06	1.60E+08	5.57E+06	1.12E+06
7.2	0.872	3.35	19.94	9.29E-02	9.50E-02	-0.097	-0.061	2.99E+06	1.37E+08	4.77E+06	8.91E+05
7.35	0.848	3.24	18.38	6.34E-02	8.17E-02	-0.098	-0.065	2.69E+06	1.14E+08	4.05E+06	6.93E+05
7.5	0.824	3.13	17.86	5.81E-02	7.49E-02	-0.095	-0.063	2.46E+06	1.11E+08	3.72E+06	6.36E+05
7.65	0.8	3.015	16	2.58E-02	6.18E-02	-0.099	-0.068	2.19E+06	8.99E+07	3.11E+06	4.76E+05
7.8	0.776	2.9	14.31	7.61E-03	5.21E-02	-0.101	-0.077	1.92E+06	7.00E+07	2.56E+06	3.38E+05
7.95	0.751	2.785	12.59	-1.86E-02	4.17E-02	-0.106	-0.091	1.64E+06	5.11E+07	2.04E+06	2.19E+05
8.1	0.726	2.67	12.17	-1.68E-02	3.76E-02	-0.103	-0.088	1.48E+06	4.94E+07	1.84E+06	1.98E+05
8.25	0.701	2.55	11.75	-1.51E-02	3.38E-02	-0.099	-0.085	1.33E+06	4.77E+07	1.66E+06	1.78E+05
8.4	0.676	2.43	11.33	-1.36E-02	3.03E-02	-0.096	-0.082	1.19E+06	4.60E+07	1.49E+06	1.59E+05
8.55	0.651	2.305	11.69	-1.49E-04	2.96E-02	-0.087	-0.065	1.13E+06	5.87E+07	1.51E+06	1.98E+05
8.7	0.626	2.18	11.01	1.49E-03	2.63E-02	-0.084	-0.062	1.01E+06	5.65E+07	1.34E+06	1.76E+05
8.85	0.601	2.06	10.57	1.32E-03	2.32E-02	-0.08	-0.06	8.92E+05	5.42E+07	1.19E+06	1.56E+05

Table 5. Breakdown of the blade mass by structural materials

Material	Mass	Blade filler option
Gelcoat	15.5 kg	
Nexus	22.8 kg	
Core (foam)	89.5 kg	
Skin (double-bias plies)	120.1 kg	
Lining (double-bias plies)	23.7 kg	
Unidirectional plies	386.8 kg	
Bond material	35.8 kg	
Inserts for hub attachment	35.5 kg	
Filler	2202.7 kg	Water
	2483.5 **kg**	Epoxy Slurry
Total blade mass	**2932.5 kg**	Water
	3213.2 kg	Epoxy Slurry